Chapter 2

Fluorescence spectroscopy of nano colloids of ZnO

Abstract

The fluorescence characteristics of nano colloids of ZnO have been studied as a function of the excitation wavelength and particle size. We have found that emission shifts with the change of the excitation wavelength. The excitation wavelength dependent shift of the fluorescence maximum is measured to be between 60 and 100 nm for a change in excitation wavelength from 230 to 355 nm. ZnO is reported to show two emission bands namely an ultraviolet (UV) emission band (380 nm) and another in the green region (530 nm). Apart from the observation of these reported emissions due to near bandgap emission and impurity related emissions, we have found some peculiar features in the fluorescence spectra that are consistent with the nanoparticle size distribution. Results reveal that additional blue emissions at 420 nm and 490 nm are developed with increasing particle size. Systematic studies on nano ZnO have indicated the presence of luminescence due to excitonic emissions when excited with 255 nm as well as significant contribution from surface defect states when excited with 325 nm. The relevant energy levels showing the transitions corresponding to the observed peaks in the emission spectrum of ZnO of particle size 18 nm under 255 nm excitation are identified. The luminescence mechanism and a correlation analysis between the particle size and spectroscopic observations are discussed.

The results of this chapter are published in
Litty Irimpan et.al., Journal of Applied Physics **102**, 063524 (2007)
Litty Irimpan et.al., Journal of Physics D: Applied Physics **40,** 5670 (2007)

2.1 Introduction

Recently, the interest on the short wavelength display device is more increasing[1]. Although laser diode or light emitting diode using GaN was already reported, ZnO has several fundamental advantages over its chief competitor, GaN: (1) its free exciton is bound with energy 60 meV, much higher than that of GaN (21–25 meV); (2) it has a native substrate; (3) wet chemical processing is possible and (4) it is more resistant to radiation damage[2]. Optical UV lasing, at both low and high temperatures, has already been demonstrated, although efficient electrical lasing must await the additional development of good *p*-type material[3]. The growth mechanisms and potential applications of these nanostructures have been reviewed by Wang[4].

The ZnO bulk or nano particles have various luminescence transitions since different preparation techniques lead to varying structures and surface properties in ZnO. Generally, ZnO exhibits two kinds of emissions: one is in the ultraviolet region corresponding to near band edge emission and the other in the visible region corresponding to deep level emissions[5-6] with a peak in the range from 450 to 730nm. Out of the different reported emission peaks, the origin of the green emission is the most controversial.

Stoichiometric zinc oxide is an insulator that crystallizes with the wurtzite structure to form transparent needle-shaped crystals. The structure contains large voids which can easily accommodate interstitial atoms. Consequently, it is virtually impossible to prepare really pure crystals. Moreover, when these crystals are heated, they tend to lose oxygen[7]. For these reasons, ZnO shows *n*-type semiconducting properties with many defects, such as lack of oxygen and the excess of zinc. It is known that visible luminescence is mainly due to defects which are related to deep level emissions, such as Zn interstitials and oxygen vacancies. Vanheusden *et al.*

found that oxygen vacancies are responsible for the green luminescence in ZnO[8]. Oxygen vacancies occur in three different charge states: the neutral oxygen vacancy (Vo^0), the singly ionized oxygen vacancy (Vo^*) and the doubly ionized oxygen vacancy (Vo^{**}) of which only Vo^* can act as the so-called luminescent center[9].

2.2 Theory

Optical properties of semiconductor nanocrystals depend on the structure of valence and conduction electronic states. One of the most interesting effects of low dimensional semiconductor quantum structures[10-13] is the size dependent bandgap. The oldest and less computationally demanding approach is the effective mass approximation (EMA) model mostly relying on infinite-well confining potentials[14, 15]. In 1990 Kayanuma and Momiji[16] introduced the finite depth square well effective mass approximation (FWEMA). Recently, a more refined method has been adopted by other researchers. It has been shown that the refined method considerably improves the model which is suitable for quantitative predictions[13, 17]. Moreover, Pellegrini et al.[18] systematically investigated the applicability and limitations of the finite depth square well effective mass approximation (FWEMA), applying it to several semiconductor quantum dots (QD) and the numerical results on these systems is obtained recently using the potential morphing method[12] (PMM). Using the PMM, the effective bandgap of colloidal QDs can be estimated using the FWEMA. FWEMA can be extended even to the case of narrow bandgap semiconductor QDs assuming a size dependent dielectric constant.

Brief description of the model described by *S Baskoutas et al.* is given below. In the effective mass approximation, the Hamiltonian for the electron–hole system contains kinetic energy of electron and hole, confinement potential for electron and hole and their coulomb interaction energy[15]. It can be written as,

$$H = -\frac{\hbar^2}{2m_e^*}\overrightarrow{\nabla_e^2} - \frac{\hbar^2}{2m_h^*}\overrightarrow{\nabla_h^2} + V_0^e\left(\vec{r_e}\right) + V_0^h\left(\vec{r_h}\right) - \frac{e^2}{\varepsilon}\frac{1}{r_{eh}} \qquad (2.1)$$

where $m_e^*\left(m_h^*\right)$ is the effective electron (hole) mass, ε is the effective dielectric constant, $r_{eh} = \left|\vec{r_e} - \vec{r_h}\right|$ is the electron–hole distance in three dimensions and $V_0^e\left(\vec{r_e}\right)\left[V_0^h\left(\vec{r_h}\right)\right]$ is the confinement potential of electron (hole). For QDs the potential is assumed to be centro-symmetric; it has a constant value $V_0^e\left[V_0^h\right]$ for distances larger than the QD radius and it vanishes inside the dot. The Bohr radius of Hydrogen atom, a_B^H and that of the electron and hole pair, a_B^{QD} are given by

$$a_B^H = \frac{h^2\varepsilon}{\pi m_e e^2} \quad and \quad a_B^{QD} = \frac{h^2\varepsilon}{2\pi\mu e^2} \qquad (2.2)$$

where μ is the effective mass and $\frac{1}{\mu} = \frac{1}{m_e^*} + \frac{1}{m_h^*}$. In order to appreciate the different Bohr radius of quantum dots (a_B^{QD}) with that of hydrogen atom (a_B^H), let us evaluate the respective numerical values.

$$a_B^H = \frac{h^2\varepsilon}{\pi m_e e^2} = \frac{\left(6.63\times10^{-34}\right)^2 \times 8.85\times10^{-12}}{3.14\times9.1\times10^{-31}\times\left(1.6\times10^{-19}\right)^2} \sim 0.5A^0$$

For ZnO, $\mu = \frac{m_e}{2}$ *and* $\varepsilon = 3.7\,\varepsilon_0$

$$a_B^{ZnO} = \frac{h^2\varepsilon}{2\pi\mu e^2} = 3.7\,a_B^H = 3.7\times0.52A^0 = 2nm$$

Charged particles, electrons and holes have two potentials: the interaction Coulomb potential and the spherical well potential that quantifies the kinetic energies of the electron-hole pair. The Coulomb energy scales as

$\frac{e^2}{\varepsilon R}$ where as electron-hole pair (e-h pair) kinetic energy in the well of radius R scales as $\frac{\hbar^2}{2\mu R^2}$. The relative importance of these two potentials enables us to distinguish three different confinement regimes.

2.2.1: Weak confinement regime ($R>>a_B$)

When the Coulomb energy is much larger than the confinement energy, the regime is called weak confinement and the particle size is much larger than Bohr radius. In this case, the e-h pair is confined as a whole and the quantification of the movement of the centre of mass is accomplished. Then the envelope wavefunction of the e-h pair is the product of two wavefunctions describing the movement of the e-h pair with respect to center of mass and the movement of the centre of mass confined in the infinite spherical well. On solving the Schrodinger equation, we get the energies of possible related optical transitions as,

$$E_n = E_g - E_{exc} + \frac{\hbar^2 \pi^2 n^2}{2MR^2} \tag{2.3}$$

where $M = m_e^* + m_h^*$ is the total mass of the e-h pair, $R = \frac{m_e^* \vec{r}_e + m_h^* \vec{r}_h}{m_e^* + m_h^*}$ is the position of the centre of mass, E_g denotes the bulk bandgap energy, E_{exc} is the exciton binding energy and n is quantum number. The energy of $(n+1)^{th}$ optical transition is,

$$E_{n+1} = E_g - E_{exc} + \frac{\hbar^2 \pi^2 (n+1)^2}{2MR^2} \tag{2.4}$$

$$E_{n+1} - E_n = \frac{\hbar^2 \pi^2}{2MR^2}(2n+1) = \frac{h^2}{4MR^2}\left(n + 1/2\right) = \alpha\left(n + 1/2\right) \tag{2.5}$$

where $\alpha = \frac{h^2}{4MR^2}$ (2.6)

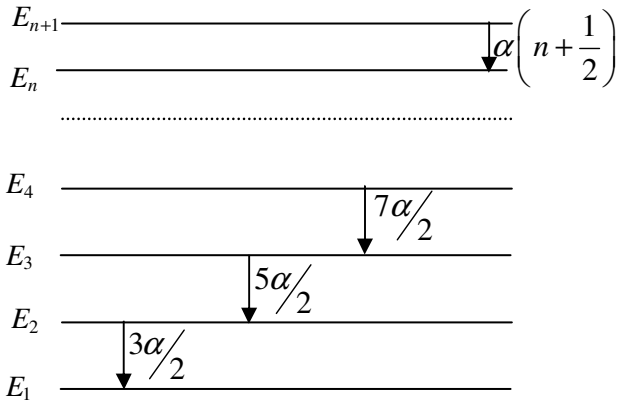

Figure 2.1: Energy level diagram of the excitons in ZnO under weak confinement regime ($R>>a_B$)

For ZnO colloids of particle size, R=18 nm,

$$\alpha = \frac{h^2}{8m_e R^2} = 1.85\times10^{-22} J = 0.0012eV = 9.6cm^{-1} \qquad (2.7)$$

When n=1, The energy of first optical transition is,

$$E_B = E_g - E_{exc} + \frac{\hbar^2\pi^2}{2MR^2} = E_g - E_{exc} + \frac{\alpha}{2} = 3.31eV \qquad (2.8)$$

where the bulk bandgap energy of ZnO is 3.37 eV and the exciton binding energy is 60 meV.

2.2.2: Strong confinement regime ($R<<a_B$)

Here the Coulomb energy is negligible with respect to confinement energy and this regime appears when the particle size is much smaller than Bohr radius. In this case, both electron and hole are confined separately. The movement of both the carriers is independent and they are considered separately confined in the infinite spherical potential. Confinement energies of the electron and hole depend only on n and l quantum numbers and can be written as

$$E_{n,l}^{e,h} = \frac{\hbar^2 \alpha_{n,l}^2}{2m_{(e,h)}^* R^2} \tag{2.9}$$

with $\alpha_{1,0} = \pi, \alpha_{1,1} \approx 1.43\pi, \alpha_{2,1} \approx 1.83\pi,$ etc…

Calculation of selection rules for dipolar transitions shows that in the optically allowed transitions, the quantum numbers n and l are preserved. By perturbation approach, the Coulomb energy is calculated and the total energy of the first optical transition, 1S-IS (n_e=n_h=1, l_e=l_h=0, m_e=m_h=0) is written as

$$E_{1S-1S} = E_g + \frac{\hbar^2 \pi^2}{2\mu R^2} - \frac{e^2}{\varepsilon}\frac{1.8}{R} \tag{2.10}$$

2.2.3: Intermediate regime (R~a_B)

Here, the Coulomb energy is no longer negligible with respect to confinement energy. In general, the electron and hole have different effective masses. The electron is the lightest particle, and only its movement is confined. To solve the problem in this situation, the results of strong confinement are taken as a departure point to diagonalize the Hamiltonian and to use a variational calculation or a perturbative calculation to take into account the Coulomb interaction.

In any case, the boundaries of the different regimes are not really strict and it is common to extend the theory of strong confinement to describe transitions near the threshold of optical absorption. The main results in the effective mass approximation (EMA) are the transformation of a band structure into a series of discrete levels for which their energy depends on nanocrystal size and increase of first optical transition energy with respect to the bulk gap energy. For very small nanocrystals, this EMA cannot be applicable since it is based on weak confinement regime. A theoretical model has been proposed by *Grigorian G B et al.* taking into account of the complexity of the electronic structure of conduction and valence bands in the strong confinement regime which gives a better result[19-23].

The Hartree-Fock formulation for two particles (electron and hole) results in the following coupled equation[24]

$$\left[\frac{\overrightarrow{p_i^2}}{2m_i^*}+U_i\left(\vec{r}_i\right)\right]\Phi_i\left(\vec{r}_i\right)=E_i\Phi_i\left(\vec{r}_i\right) \tag{2.11}$$

where *i*=e or h and the e and h indices refer to the electron and the hole, respectively. The self-consistent effective field *Ui*(*ri*) that acts on the electron is given by

$$\begin{aligned}U_e\left(\vec{r}_e\right)\Phi_e\left(\vec{r}_e\right)=&\left[V_0^e\left(\vec{r}_e\right)-\frac{1}{2}\frac{e^2}{\varepsilon}\int d\vec{r}_h\frac{\left|\Phi_h\left(\vec{r}_h\right)\right|^2}{\left|\vec{r}_e-\vec{r}_h\right|}\right]\Phi_e\left(\vec{r}_e\right)\\&+\frac{1}{2}\frac{e^2}{\varepsilon}\int d\vec{r}_h\frac{\Phi_h^*\left(\vec{r}_h\right)\Phi_e\left(\vec{r}_h\right)}{\left|\vec{r}_e-\vec{r}_h\right|}\Phi_h\left(\vec{r}_e\right)\end{aligned} \tag{2.12}$$

while the self-consistent effective field that acts on the hole takes the form

$$\begin{aligned}U_h\left(\vec{r}_h\right)\Phi_h\left(\vec{r}_h\right)=&\left[V_0^h\left(\vec{r}_h\right)-\frac{1}{2}\frac{e^2}{\varepsilon}\int d\vec{r}_e\frac{\left|\Phi_e\left(\vec{r}_e\right)\right|^2}{\left|\vec{r}_e-\vec{r}_h\right|}\right]\Phi_h\left(\vec{r}_h\right)\\&+\frac{1}{2}\frac{e^2}{\varepsilon}\int d\vec{r}_e\frac{\Phi_e^*\left(\vec{r}_e\right)\Phi_h\left(\vec{r}_e\right)}{\left|\vec{r}_h-\vec{r}_e\right|}\Phi_e\left(\vec{r}_h\right)\end{aligned} \tag{2.13}$$

In order to solve the iterative Hartree-Fock equations, the potential morphing method is applied, using the three-dimensional harmonic oscillator as reference system. Once the Hartree-Fock iteration scheme converges, the total energy of the exciton is estimated by the following expression

$$E\left(X\right)=E_e+E_h \tag{2.14}$$

and the corresponding effective bandgap is given by

$$E_g^{eff}\left(X\right)=E_g+E\left(X\right) \tag{2.15}$$

As a first order approximation, the electrons and the holes are assumed to be confined by the same finite square well potential in three-dimensions[18]. The form of the lateral confinement potential is (where the indices for both electrons and holes are omitted)

$$V_0^{e(h)}\left(r_{e(h)}\right)=0,\ \ r_{e(h)}\le R \\ =V_0,\ \ r_{e(h)}>R \tag{2.16}$$

where R is the QD radius and $\overrightarrow{r_{e(h)}}=\left(x_{e(h)},y_{e(h)},z_{e(h)}\right)$ is the three dimensional position vector of the electron (hole). The height of the finite depth well confining potential is independent of the specific type of the semiconductor QD and depends exclusively on the matrix energy bandgap by a simple linear relation of the form

$$V_0=0.08E_g\left(M\right) \tag{2.17}$$

where $E_g(M)$ is the matrix energy bandgap. The material parameters used in the potential morphing method calculations for ZnO such as effective masses and dielectric constants are $\frac{m_e^*}{m_e}=0.24,\frac{m_h^*}{m_e}=0.45 and \varepsilon=3.7$.

Thus the energy shift of the optical absorption edge is size dependent and luminescence experiments give complementary information. The red shift in bandgap fluorescence with particle size closely follows the red shift in the absorption band edge. When particle size decreases, the overlap of the electron and hole wavefunctions increase and the Coulomb interaction between particles also increases. If two or more e-h pairs are present in the nanocrystal, a phenomenon known as Auger ionization becomes important. Theoretical treatment of this process is complex[25]. Auger effect efficiency is related to e-h pair Coulomb interaction. Auger ionization consists of an energy transfer from one e-h pair, which relaxes non-radiatively, to the other pair in the nanocrystal. Then the ejection of an

electron or a hole belonging to the second pair to the surrounding matrix occurs and the lifetime of e-h pairs become shorter and shorter as the number of e-h pairs increases for a given size. As the particle size decreases, the electronic confinement increases the Coulomb interaction and decreases lifetime. For example, the fluorescence life time of CdSe nanocrystal is reported to be reduced from 360ps to 6ps when the particle size reduces from 4.1 nm to 1.2 nm[26]. This reduction in fluorescence lifetime leads to excitation wavelength dependent emission behaviour in nanocrystals. This behaviour is less important in semiconductors with large particle size because of the reduction in e-h interaction and because of the restrictions imposed by energy and momentum conservation.

2.3 Synthesis of nano colloids of ZnO

ZnO is prepared by two different chemical routes and different capping agents like Poly Vinyl Pyrrolidone(PVP) and Poly Ethylene Imine(PEI) have been used.

2.3.1 Polyol method

In the present investigation, colloids of ZnO are synthesized by a modified polyol precipitation method[27-30]. The monodisperse ZnO colloidal spheres are produced by a two-stage reaction process. The method of preparation involves the hydrolysis of zinc acetate dihydrate (ZnAc) in diethylene glycol medium (DEG). Among the different polyols, diethylene glycol (DEG) is chosen because it is reported to give particles with uniform shape and size distribution. The size of the particles and hence the stability of this colloidal suspension depend on the concentration of zinc acetate as well as on the rate of heating. The molar concentration of precursor solution is varied from 0.01mM to 0.1M and a heating rate of 4^{o}C per minute is employed for the formation of ZnO at a temperature of 120^{0}C. The product from the primary reaction is placed in a centrifuge and the supernatant (DEG, dissolved reaction products, and unreacted ZnAc and water) is decanted off

and saved. A secondary reaction is then performed which is similar to the above procedure to produce the monodisperse ZnO spheres. Prior to reaching the working temperature, typically at 115^0C, some volume of the primary reaction supernatant is added to the solution. After reaching 120^0C, it is stirred for one hour, to get a monodisperse stable colloid.

2.3.2 Capping

In the second method that we adopted, 1mM zinc acetate is dissolved in isopropyl alcohol (IPA-Merck, HPLC grade) by stirring at 50^0C in the presence of capping agent poly vinyl pyrolidone (PVP-Sisco)[30]. ZnO colloid is formed when it is hydrolysed with sodium hydroxide under ultrasonification for 2 hours. In the third method, we used another cationic dispersant poly ethylene imine (PEI- Sigma Aldrich] as capping agent[31]. PEI is a polyelectrolyte and it makes the surface positively charged. The positive charges keeps the particles repelled from each other and prevent agglomeration. The long polymeric chains of PEI on the other hand effectively cap the surface as soon as nucleation occurs and prevents growth. Thus, a polyelectrolyte can make a stable nano semiconductor crystal colloid by these two mechanisms.

2.4 Absorption spectroscopy of nano colloids of ZnO

The ZnO colloids are characterized by optical absorption measurements recorded using a spectrophotometer (JascoV-570 UV/VIS/IR). Figure 2.2 gives the room temperature absorption spectra of the ZnO colloids prepared by polyol method. The excitonic peak is found to be blue shifted with decrease in particle size (370-350 nm) with respect to that of bulk ZnO (395 nm) and this could be attributed to the confinement effects[32].

In the case of nanocrystallites, the electrons, holes and excitons have limited space to move and their limited motion becomes possible only for definite values of energy. The highest occupied valence band and lowest unoccupied conduction band are shifted to a more negative and positive

values respectively resulting in widening of bandgap. This leads to a blue shift of absorption band which can be observed through optical absorption and transmission studies. This size dependent shifts in absoption band edge are shown in figure 2.2. From the figure, it is clear that ZnO colloids of size 4.5 nm to 6 nm lies in one regime called intermediate regime ($R \sim a_B$) and ZnO colloids of size 10 nm to 18 nm lies in the other regime called weak confinement regime ($R > a_B$).

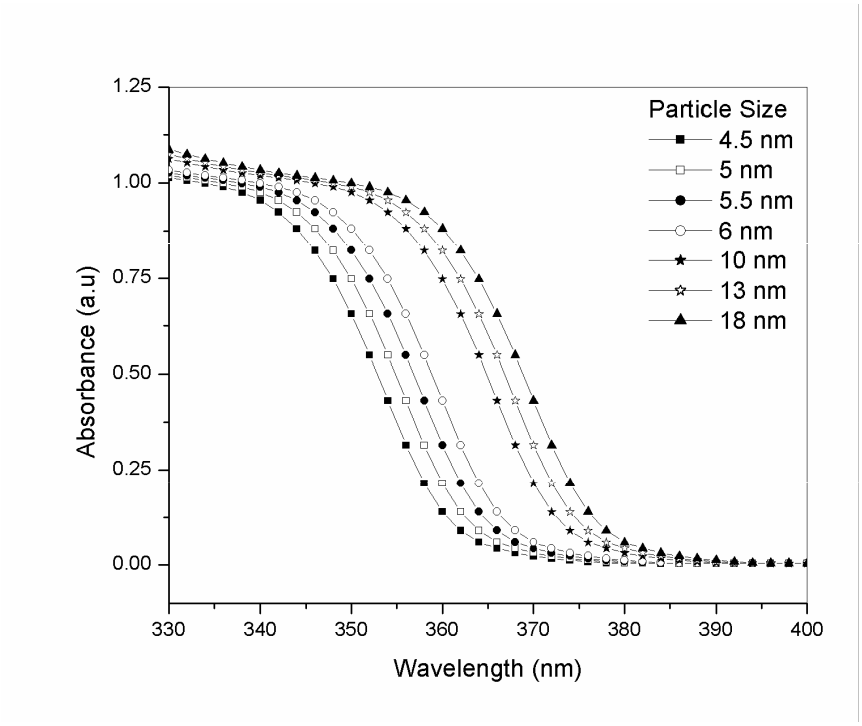

Figure 2.2: Size dependent absorption spectroscopy of ZnO colloids prepared by modified polyol method

The pronounced dependence of the absorption bandgap on the size of ZnO nano crystals is used to determine the particle size. The cluster sizes are calculated from the absorption spectra using the analytical formula given by Ranjani Viswanatha et al[33]. To get a precise measure of the shift, the first

derivative curve of the absorption spectrum is taken and the point of inflection is taken as the cut-off wavelength and is shown in figure 2.3.

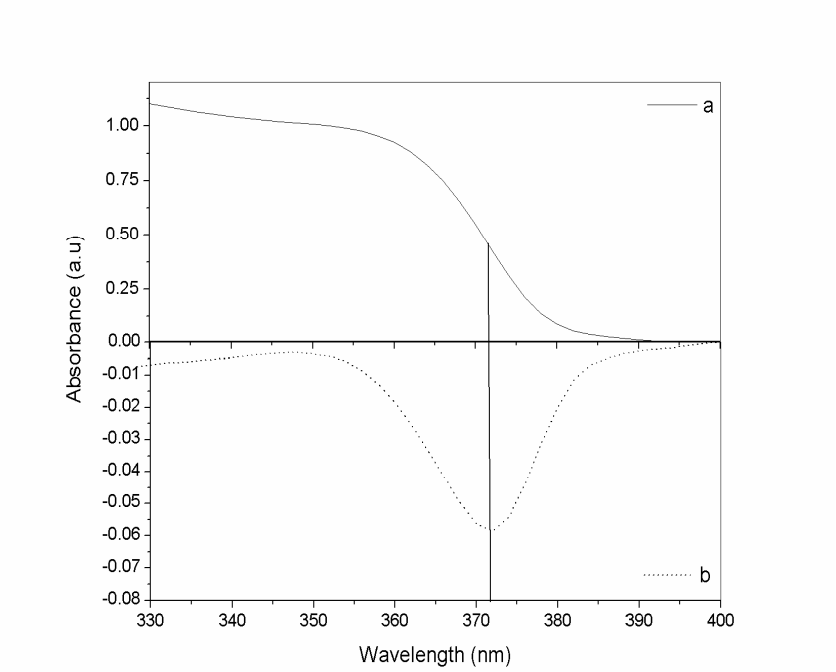

Figure 2.3 (a): Absorption spectrum (b): first derivative of the absoption spectrum of ZnO colloids of size 18 nm.

From the cut-off wavelength, the corresponding E_g is calculated. The deviation of this from the E_g of bulk ZnO gives ΔE_g and the particle size, d is determined using the equation,

$$\Delta E_g = 100\left(18.1d^2 + 41.4d - 0.8\right)^{-1} \qquad (2.18)$$

Figure 2.4 gives the room temperature absorption spectra of the ZnO colloids prepared by different chemical routes in which the effect of capping is clearly seen.

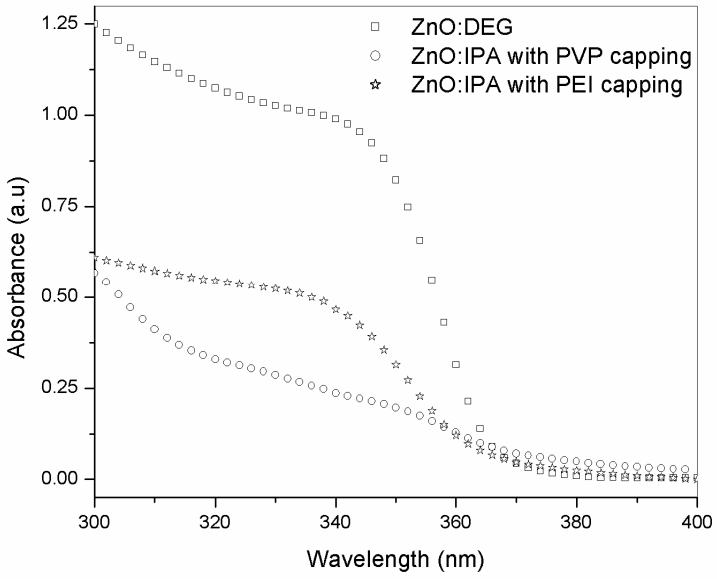

Figure 2.4: Absorption spectra of the ZnO colloids prepared by different chemical routes

2.5 X-ray diffraction (XRD)

The powder extracted from the colloid of large particle size is characterized by x-ray diffraction. Typical XRD pattern of ZnO colloid is given in figure 2.5. The diffraction pattern and interplane spacings can be well matched to the standard diffraction pattern of wurtzite ZnO, demonstrating the formation of wurtzite ZnO nanocrystals[34]. The particle diameter d is calculated using the Debye–Scherer formula

$$d = \frac{0.89\lambda}{\beta \cos\theta} \tag{2.19}$$

where λ is the x-ray wavelength (1.5406 Å), θ is the Bragg diifraction angle, and β is the peak width at half maximum[35]. The XRD peak at 36° in

figure 2.5 gives the ZnO particle diameter of 18 nm and matches well with the size calculated from absorption spectrum.

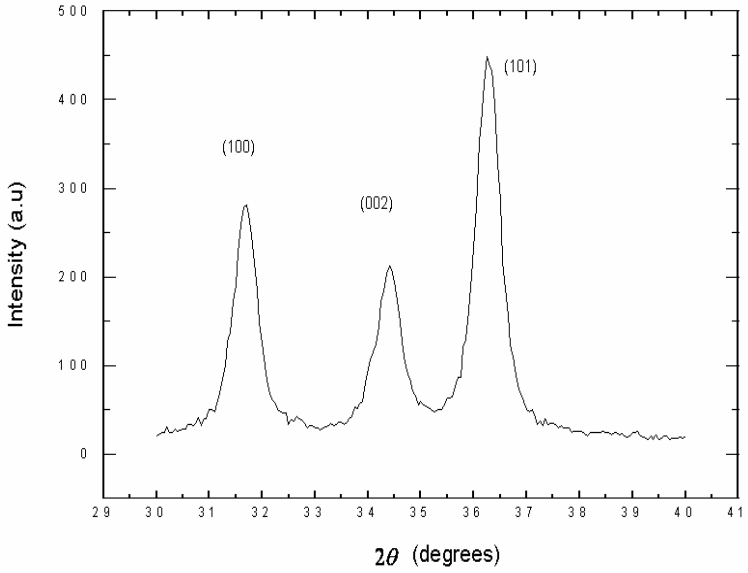

Figure 2.5: XRD pattern of the powder extracted from ZnO colloid of size 18 nm

2.6 Optical bandgap

The absorption of a photon, leading to excitation of an electron from the valence band to the conduction band, is associated with the bandgap energy. The direct bandgap of ZnO colloids are estimated from the graph of $h\nu$ vs $(\alpha h\nu)^2$ for the absorption coefficient α which is related to the bandgap E_g as $(\alpha h\upsilon)^2 = k(h\upsilon - E_g)$, where $h\nu$ is the incident light energy and k is a constant. Extrapolation of the linear part until it intersects the $h\nu$ axis gives E_g. The optical bandgap (E_g) is found to be size dependent and there is an increase in the bandgap of the semiconductor with a decrease in the particle size as shown in figure 2.6.

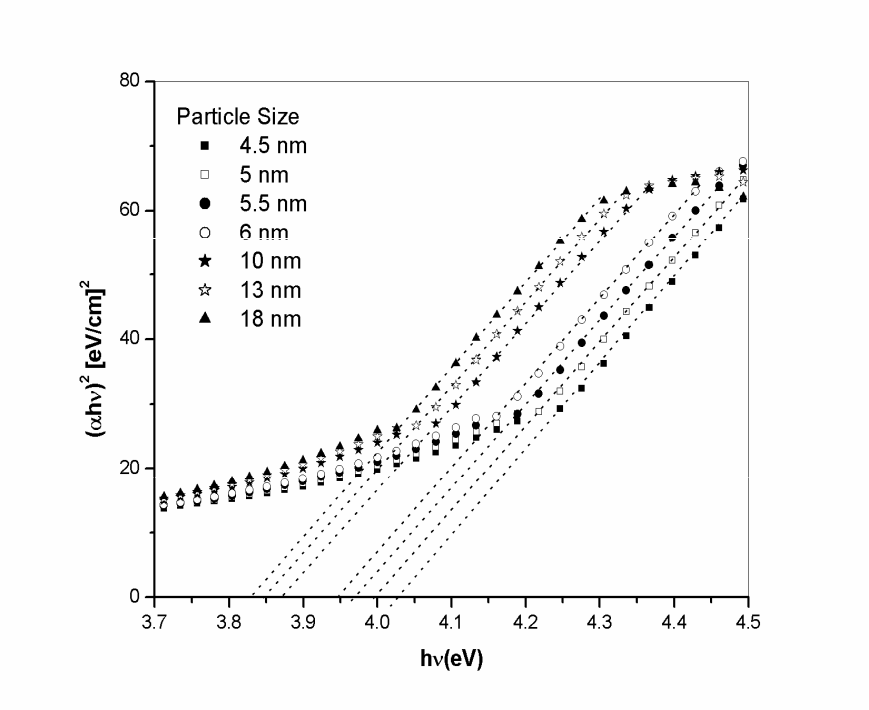

Figure 2.6 : Optical bandgap of ZnO colloids

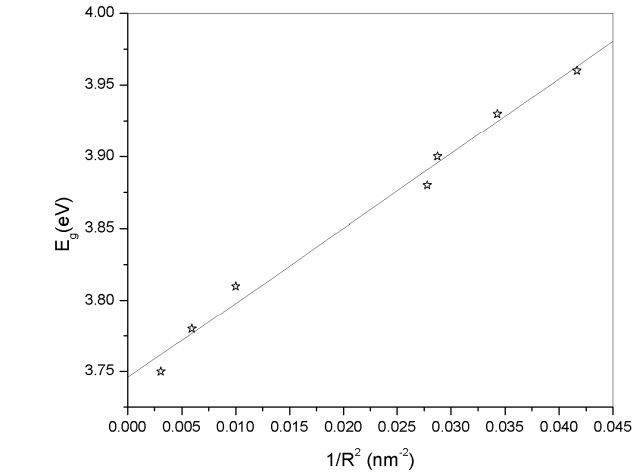

Figure 2.7: Variation of optical bandgap as a function of $1/R^2$

Figure 2.7 shows the optical bandgap energy as a function of $1/R^2$. The bandgap energy becomes larger with decreasing size. This effect is considered to be due to confinement of the exciton in the nanocrystal. When we apply equation (2.3) the y-intercept gives $E_B=E_g-E_{exc}=3.75eV$ which is comparable with the theoretical value in equation (2.8).

The total change in the bandgap of the material is jointly contributed by shifts of the valence and the conduction band edges away from each other and is schematically shown in figure 2.8. In general, the shift of the top of the valence band (TVB) is not the same as that of the bottom of the conduction band (BCB). Moreover, there are recent studies, though few in number,[36] that report the individual shifts in top of the valence band and bottom of the conduction band as a function of the size employing various forms of high-energy spectroscopies, such as the photoemission and the x-ray absorption spectroscopies.

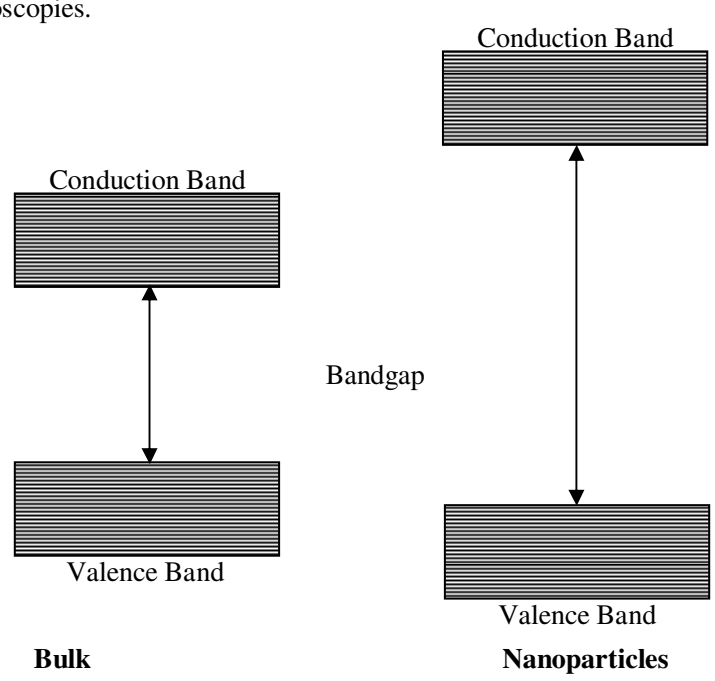

Figure 2.8: Schematic representation of bandgap in bulk and nanoparticles

Thus, it is desirable to compute these shifts of the individual band edges with the size of the nanocrystallite. The shifts of the band edges decrease smoothly to zero for large sized nanocrystals in every case and the shift in the bottom of the conduction band is in general much larger compared to the shift in the top of the valence band for any given size of the nanocrystal. This indicates that the shifts in the total bandgap as a function of the nanocrystal size are always dominated by the shifts of the conduction band edge in these systems.A larger shift for the bottom of the conduction band is indeed expected in view of the fact that the band-edge shifts are related inversely to the corresponding effective masses[5] and the effective mass of the electron is always much smaller than that of the hole in these II-VI semiconductors. From this band edge shifts, the electronic structure as a function of the nanocrystallite size can be calculated for semiconductors[37]. The bandgap is found to be in the range 3.5-4 eV for the range of particles from 4.5-18 nm which is in agreement with the reported value[38].

2.7 Fluorescence spectroscopy

The fluorescence emission from ZnO colloids is recorded using a Cary Eclipse fluorescence spectrophotometer (Varian). The fluorescence behaviour of nano colloids of ZnO has been studied as a function of the excitation wavelength and particle size. The reduction in fluorescence lifetime with decrease in particle size leads to excitation wavelength dependent emission behaviour in nanocrystals. This behaviour is less important in semiconductors with large particle size because of the reduction in electron-hole interaction and because of the kinetic restrictions imposed by energy and momentum conservation.

2.7.1 Excitation spectrum

Figure 2.9 shows the excitation spectrum corresponding to the emission peak at 390 nm and exhibiting two excitation wavelengths at

$\lambda_{ex}^{(1)}$=255 nm and $\lambda_{ex}^{(2)}$=325 nm. Since ZnO has a broad band absorption, excitation spectrum is very significant in finding the excitation wavelengths at which it has maximum emission.

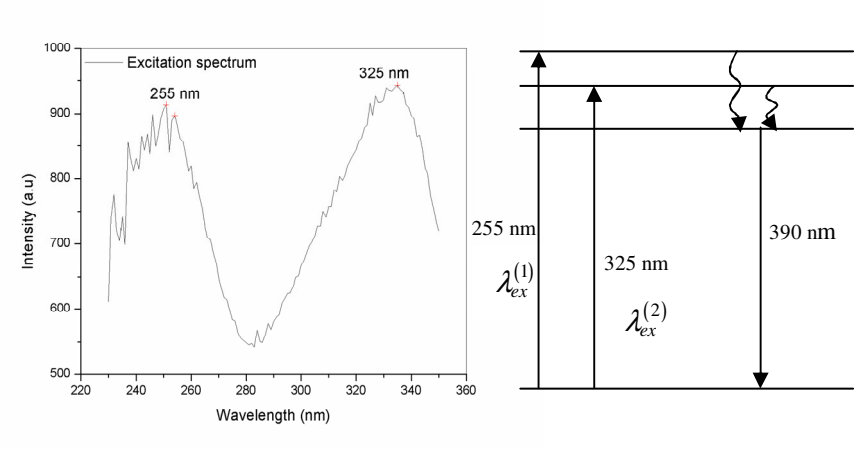

Figure 2.9: Excitation spectrum of ZnO colloid for an emission peak of 390 nm

2.7.2 Excitation wavelength dependent fluorescence spectroscopy

The steady state absorption and fluorescence behaviour of nano colloids of ZnO, in which spectra are sensitive to the polarity of the surrounding environment, has been studied with a view to obtaining information on how the polarity of these liquids influence the fluorescence behaviour. Time-resolved fluorescence studies on dipolar solutes, which have revealed wavelength dependence of the fluorescence decay profiles and dynamic fluorescence Stokes shift in the ps–ns time scale[39-42], have thrown insight into the mechanism of solvation. The excitation at the tail of the absorption band gives rise to an emission that shifts with the change of the excitation wavelength[43]. This kind of excitation wavelength dependent fluorescence behaviour has also been reported for some dipolar solutes in ionic liquids[44]. The excitation wavelength dependent emission behaviour of

nano colloids of ZnO is considered unusual as the literature suggests that ZnO does not exhibit excitation wavelength dependent behaviour[6, 45] and the observed behaviour is contrary to what is prescribed by the well-known Kasha's rule of excitation wavelength independence of the emission spectrum[46] (figure 2.10).

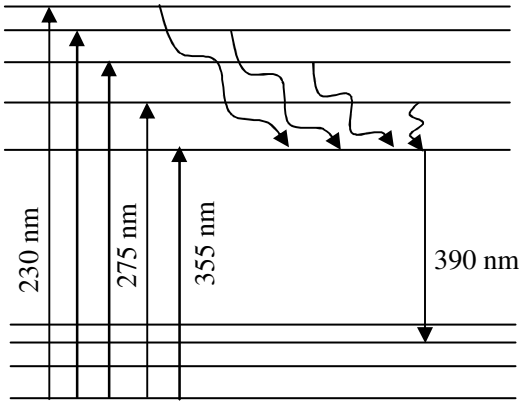

Figure 2.10: Schematic representation of Kasha's rule of excitation wavelength independence of the emission spectrum

To understand the origin of this behaviour, we have undertaken the present investigation on nano ZnO colloids prepared in two different media of different viscosities. The behaviour of these systems that show excitation wavelength dependent fluorescence spectra is also examined by capping them with two different capping agents. Figure 2.11 shows the excitation wavelength dependent fluorescent behaviour in nano colloids of ZnO prepared by polyol method. When ZnO prepared in diethylene glycol medium is excited at the UV side (say, at 230-240 nm) of the absorption maximum, the fluorescence maximum (λ_{em}^{max}) of ZnO is observed at 346 nm. Interestingly, as can be seen from figure 2.11, as the excitation wavelength is progressively shifted towards the red side, there is a shift in the fluorescence

maximum. The shift in the fluorescence maximum is small and steady when the excitation wavelength changes from 275 nm to 325 nm whereas the shift is significant when the excitation wavelength varies near the edge of $\lambda_{ex}^{(1)}$ and $\lambda_{ex}^{(2)}$.

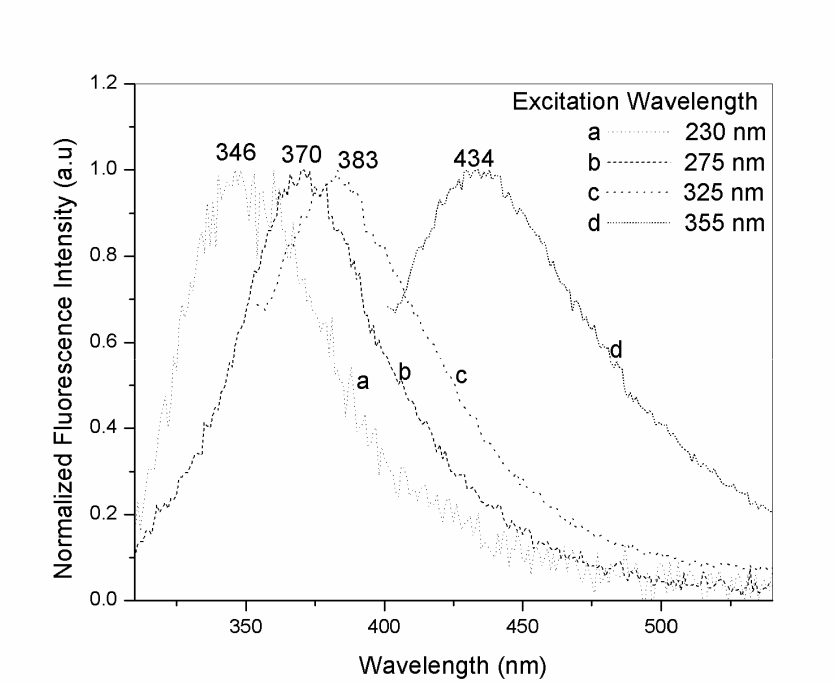

Figure 2.11: Normalized fluorescence spectra of ZnO nano colloids of size 6 nm as a function of excitation wavelength. The fluorescence spectra have been corrected for the instrumental response.

The dependence of λ_{em}^{max} of ZnO of different particle size prepared by polyol method on the excitation wavelength (λ_{ex}) is shown in figure 2.12. The extent of the shift, as measured from λ_{em}^{max}, is around 90 nm for the range of excitation wavelength studied.

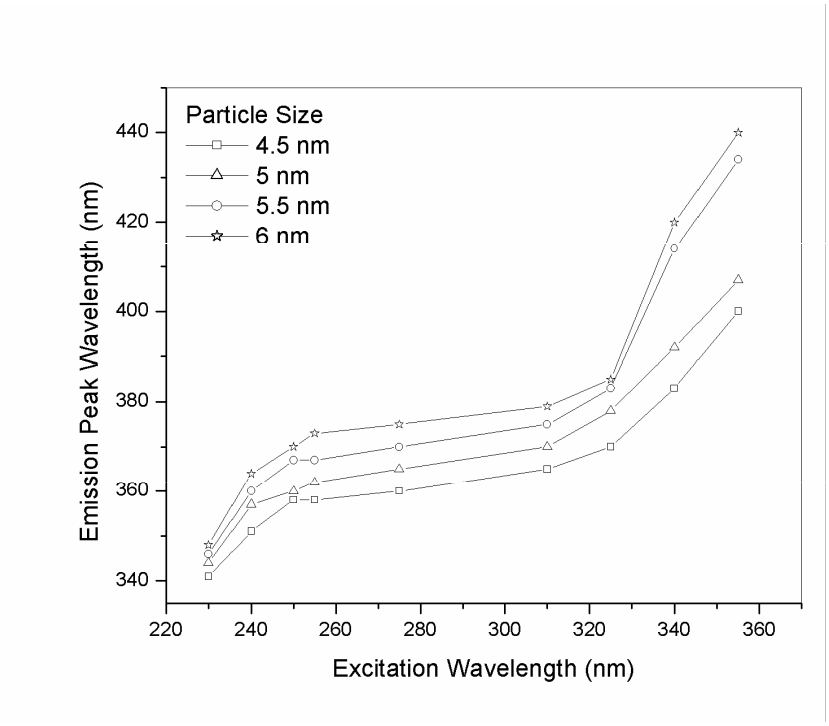

Figure 2.12: λ_{em}^{max} *vs* λ_{ex} *plots of nano colloids of ZnO of different sizes prepared by modified polyol synthesis*

Figure 2.13 shows the dependence of λ_{em}^{max} on the excitation wavelength of nano colloids of ZnO prepared in different media by using different capping agents. The excitation wavelength dependence of emission maxima is different for colloids prepared in different media. Although both the absorption and emission band positions are dependent on the polarity of the medium, the fluorescence spectrum is much more sensitive to the medium than the absorption spectrum. This is evident from the fact that, when the solvent is changed from isopropyl alchohol to polar diethylene glycol, the absorption maximum shifts by only 7-8 nm, whereas the emission maximum shifts by more than 20 nm. This behaviour is suggestive of an

emitting state that is more polar than the ground state. The shift remains the same when we change the capping agent in the same medium. ZnO exhibits more pronounced excitation wavelength dependence in relatively more viscous and more polar diethylene glycol medium compared to isopropyl alchohol medium. Viscosity and polarity of the medium plays a major role in the excitation wavelength dependent shift of emission maxima.

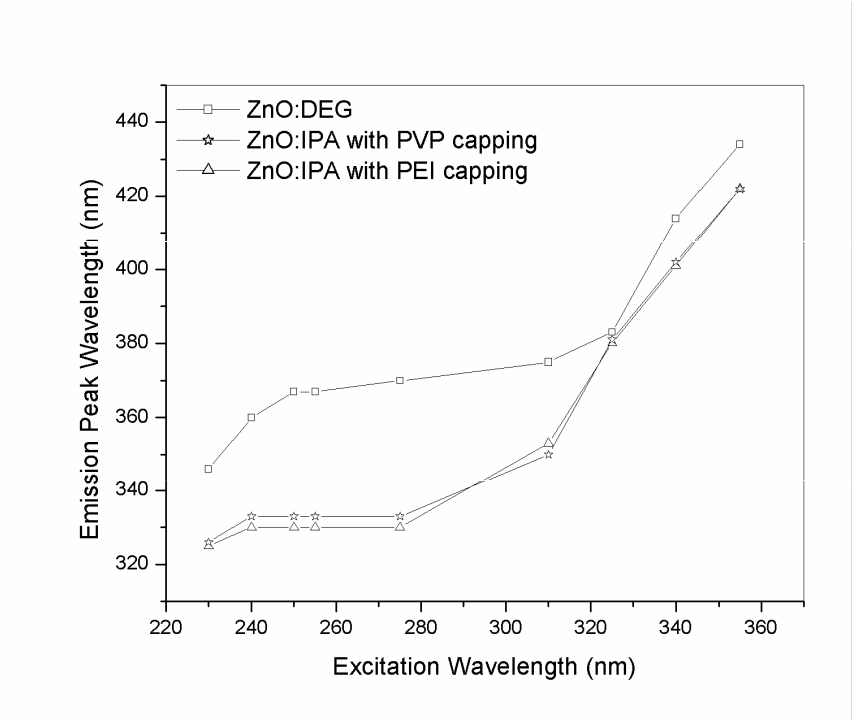

Figure 2.13: λ_{em}^{max} *vs* λ_{ex} *plots of nano colloids of ZnO prepared in different media using different capping agents*

To the best of our knowledge, this is the first report on the excitation wavelength dependent emission behaviour in nano colloids of ZnO. When the homogeneous nature of the ZnO colloids and the literature data of fluroscence emission behaviour already studied are taken into consideration,

the present observation appears to be quite unusual. However, when excited at the long wavelength edge of the first absorption band, a red shift of λ_{em}^{max} of the dipolar molecules is often observed in low-temperature glasses; polymer matrixes; and organized assemblies such as micelles, vesicles, proteins, and membranes[47, 48]. This is primarily due to the fact that (i) the probe molecules absorbing at the red edge of the absorption band have greater interaction with the solvent molecules than those absorbing in the blue side and (ii) the inhomogenous broadening can only be probed at the red excitation edge where the excitation to the higher vibrational levels does not interfere with this selection. This phenomenon is termed as the "red-edge effect" (REE)[49,50]. This is also called the edge excitation shift (EES)[48] or the edge excitation red shift (EERS)[51, 52] or the red-edge excitation shift (REES)[53, 54]. We prefer to use the REE terminology, as there is red shift in emission peak with respect to excitation wavelength and this happens to be the first accepted abbreviation for the observed phenomenon[49, 50].

2.7.3 Factors contributing to REE

The excitation wavelength dependence can arise when there exists a distribution of the molecules in the ground state that differ in their solvation sites and, hence, their energies. This inhomogeneity can originate from the difference in the interaction energies between the medium and the nano particles. However, the presence of an ensemble of energetically different molecules in the ground state *alone* does not guarantee an excitation wavelength dependent fluorescence behaviour because rapid relaxation of the excited state, such as the solvation of the fluorescent state or energy transfer between the energetically different excited states of the molecules, is expected to result in emission from the lowest energy state irrespective of the excitation. It is only when a system allows selective excitation of the

energetically different species and the relaxation of the fluorescent state is slow (hence, incomplete) that REE can be expected.

Since inhomogeneous broadening, which dictates photo-selection of the energetically different species, is directly proportional to the change of dipole moment ($\Delta\mu$) due to electronic excitation, the probe molecules with large $\Delta\mu$ values are the most suitable candidates to exhibit REE. The change in the dipole moment of ZnO upon electronic excitation is reported to be high[55].The second factor, which is even more important than the first, is that ZnO has a rather short fluorescence lifetime (τ_f). The bandgap fluorescence of ZnO has an extremely short lifetime which is reported to be 100 ps[56]. On the other hand, recent studies on solvation dynamics suggest that solvation is a rather slow process[57]. The solvent relaxation time (τ_{sol}) of the medium is of the order of nanoseconds. Because τ_{sol} around the photoexcited molecule is an order of magnitude higher than the τ_f value, it is not difficult to understand why unrelaxed fluorescence, which gives rise to the excitation wavelength dependent emission behavior, could be observed in the case of nano colloids of ZnO. When the τ_f values are higher than the τ_{sol} value of the solvent, the fluorescence occurs from a fully solvated state. Potentially, lifetime shortening with decrease in particle size has been recently found in KrN clusters[31]. This model also explains why the more short wave emission with a shorter lifetime originates from smaller clusters. Due to the low concentration of ZnO colloids of small particle size, the energy transfer between the upper vibrational level and the lower vibrational level of the excited state of these particles is inefficient owing to short fluorescence lifetime and thus the emission characteristics changes with excitation wavelength.

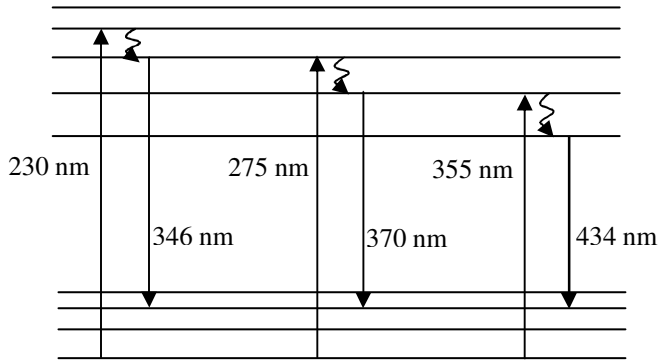

Figure 2.14: Schematic representation of excitation wavelength dependence of emission spectrum

Probe molecules with short fluorescence lifetimes are more likely to exhibit REE than those with long lifetimes. The larger the polarity and nuclear polarizability of the medium, the stronger is the interaction of the probe molecule with the solvent and higher is the chance to observe REE. The more viscous is the medium, the slower is the excited state relaxation process (intramolecular) and higher is the possibility to observe REE. The molecule fluoresces efficiently and the quantum yield increases strongly with increase in viscosity. This dependence of the fluorescence yield on viscosity and polarity has been studied previously[58]. The viscosity and possibly hardness of the medium plays a dominant role in the fluorescence efficiency of the molecule. These data can be understood by considering the effect of viscosity on the rotation of the active molecule. When these levels (modes) are hindered because of the increase in the viscosity, the rates of rotation and vibration decrease with the eventual cessation of several modes of rotation and vibration in viscous medium and solid matrices. This decrease in the active modes leads to a weaker coupling of the excited electronic states with upper levels of the ground state, which results in a decrease in the energy dissipation rate of the excited state by means of internal radiationless

channels to the ground states. Consequently the rate of population decay via radiative transitions increases and there is higher possibility to observe REE. Thus the high viscosity of the medium and short fluorescence lifetime, which makes the relaxation of the photo-excited species inefficient, contributes to REE-like behaviour in nano colloids of ZnO with smaller particle size.

The excitation wavelength dependent emission behaviour in nano colloids of ZnO is not due to any specific interaction between the medium and ZnO, but is due to incomplete solvation of the fluorescent state in the viscous medium. This is evident from the fact that ZnO exhibits shift of the λ_{em}^{max} in two media prepared by different methods. Therefore, it can be concluded that it is the incomplete solvation (relaxation) in these viscous media that is primarily responsible for the excitation wavelength dependent spectral shift of nano colloids of ZnO.

In the case of ZnO, the electrostatic interaction is expected to dominate the other interactions and probably plays the most important role in creating a distribution of energetically different molecules in the ground state that allows their photo-selection. Two factors responsible for the slow relaxation of the excited state are the retardation of solvation due to the electrostatic forces induced by charged ZnO and/or an inefficient energy transfer between the energetically different species. In the absence of any literature data on solvation dynamics, it is not possible to pinpoint at this stage whether one or both the factors contribute to REE in ZnO. Further studies, both theoretical and experimental, need to be carried out to obtain insight into this aspect. Regarding excited state relaxation, an inefficient energy transfer between the energetically different molecules takes place which presumably contributes to the excitation wavelength dependent fluorescence behaviour in this case. Thus we can conclude that the larger viscosity of the medium which slows down the excited state relaxation

process and the reduction in fluorescence lifetime due to small particle size are responsible for the excitation wavelength dependent spectral shift in nano ZnO colloids.

2.7.4 Size dependent fluorescence spectroscopy

The fluorescence spectra of nano ZnO colloids of different particle size for an excitation wavelength of 255 nm are shown in figure 2.15. Results show that additional emissions at 420 nm and 490 nm are developed with increase in particle size along with known bandgap emissions at 380 nm and impurity dominated emissions at 530 nm. The excitons can exhibit excited states, in addition to their ground state transitions which results in the additional emission peaks.

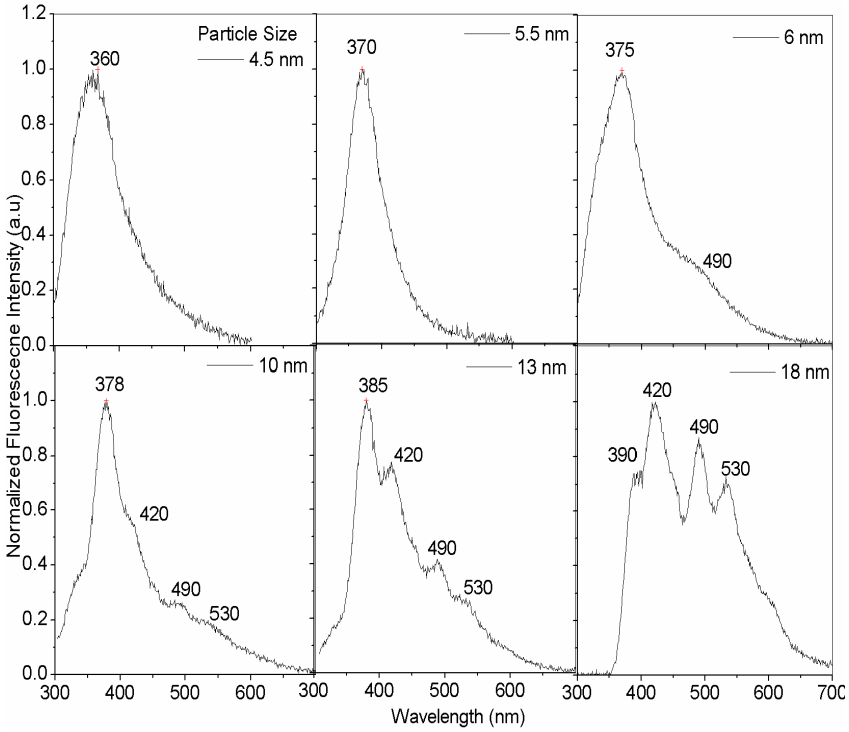

Figure 2.15:Steady state fluorescence spectra of nano ZnO colloids of different particle size for an excitation wavelength of 255 nm

Figure 2.16 shows the fluorescence spectrum of the powder extracted from ZnO colloid of 18 nm at an excitation wavelength of 255 nm. It exhibits all the characteristic emission peaks of the colloid. It confirms the fact that the emission peaks are of pure ZnO and there are no solvent effects. Figure 2.15 and 2.16 show multiple emission peaks at larger particle size. These may be attributed to transition from various excited state energy levels of exciton to the ground level corresponding to $R>>a_B$ case.

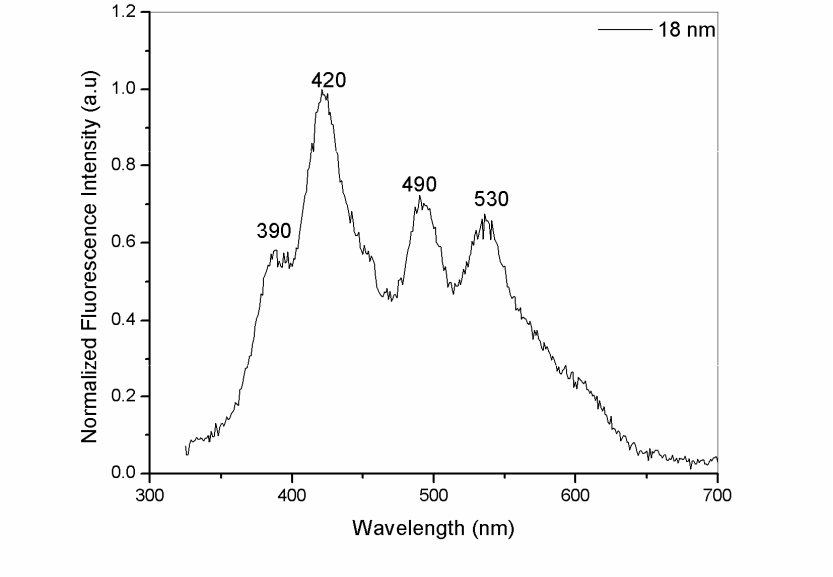

Figure 2.16: Fluorescence spectrum of the powder extracted from ZnO colloid of size 18 nm at an excitation wavelength of 255 nm

For ZnO colloids of particle size 18 nm, we get emission peaks at 390 nm, 420 nm, 490 nm and 530 nm. Additional shoulders at 455 nm, 570 nm and 600 nm are present along with the emission peaks. This series of peaks can be modelled as a particle in a box problem. Assume that the emission peak at 600 nm (2 eV) results from the transition from a higher

energy level corresponding to quantum number n to the lowest one corresponding to n=1. From equation (2.3), transition energy from n to 1 is

$$E_n - E_1 = \frac{\hbar^2\pi^2}{2MR^2}\left(n^2-1\right) = \frac{h^2}{2\times 4MR^2}\left(n^2-1\right) = \frac{\alpha}{2}\left(n^2-1\right) \qquad (2.20)$$

Therefore, $\frac{\alpha}{2}\left(n^2-1\right) =$ 2 eV and n=59. Thus 600 nm transition corresponds to n=59 to n=1 level. Similarly for other emission peaks, transitions are identified based on this model and is shown in figure 2.17.

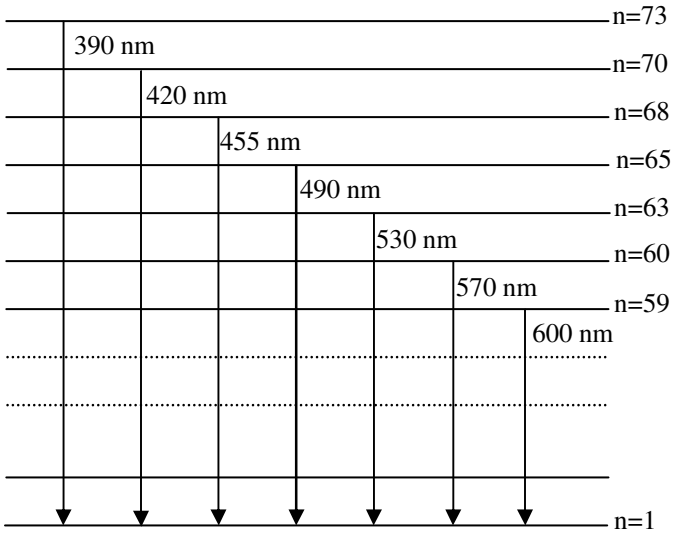

Figure 2.17: Relevant energy level diagram showing the transitions corresponding to the observed peaks in the emission spectrum of ZnO of particle size 18 nm under 255 nm excitation.

The results obtained support the fact that exciton levels in the weak confinement regime can be modelled as those related to particle in a box. The spectra are not of sufficient resolution to get the transition peaks from all the consecutive energy levels.

2.7.5 UV emission

The UV emission band is assigned to a direct *bandgap* transition. Like the absorption spectrum, this UV band undergoes a red shift with particle size. Such size dependent optical properties of semiconductor particle suspensions in the quantum regime are well known and similar observations have previously been made for several quantum particle systems[5]. For the intrinsic luminescence of ZnO nanoparticles, it is generally known that the formation of nanoparticles causes a red shift in the PL spectra due to quantum size effect[59]. An analytical approximation for the lowest eigenvalue (i.e., the first excited electronic state) is described as follows[5]:

$$E^* = E_g + \frac{h^2}{8R^2}\left(\frac{1}{m_e} + \frac{1}{m_h}\right) - \frac{1.8e^2}{\varepsilon R} + \textit{smaller terms,} \quad (2.21)$$

where E_g is the bandgap, R is the radius of the ZnO nanaoparticles, h is Plank's constant, $m_e = 0.24m_0$ is the electron effective mass, $m_h = 0.45m_0$ is the hole effective mass, ε is the dielectric constant of ZnO with an accepted value of 3.7. Results show that the fluorescence emission peak shifts from 360 nm to 370 nm as the particle size increases from 4.5nm to 6 nm as is evident from the above equation. The emission around 360 nm (3.4 eV) shown in the figure 2.14 is consistent with the bandgap of the ZnO nanoparticles. A red shift of UV emission is observed with the increase in the particle size which is attributed to quantum size effects.

With the increase in the particle size, the energy of UV luminescence is shifted from 3.5 eV (350 nm) to 3 eV (390 nm). The shift of bandgap energy is related to the structural property. Therefore, the energy of UV emission known as near band edge emission is decreased from 3.5 to 3 eV. The bandgap is found to be in the range 3.5-4 eV for the range of particles from 4.5-18 nm as shown in figure 2.5. The optical bandgap is shifted from 3.5 to 4 eV for different particle size and the shift is consistent

with the result of PL in the range of UV. The UV emission is shifted from 3.5 to 3 eV by the shift of optical bandgap from 4 to 3.5 eV and it clearly indicates that the origin of UV emission is the near band edge emission[29].

Mean cluster size could be principally derived from the absorption measurements and the enlargement effects are expected to be predominant when the particle size is less than about 6 nm as shown in figure 2.18 (a) where the band enlargement is plotted as a function of the average particle size. Figure 2.18 (b) shows the energy of the band to band transition as a function of the mean particle size. The red shift in the UV emission with particle size closely follows the red shift in the band edge, indicating that the two are related. The reconstructed size distribution curve from the fluorescence spectrum is shown below[29].

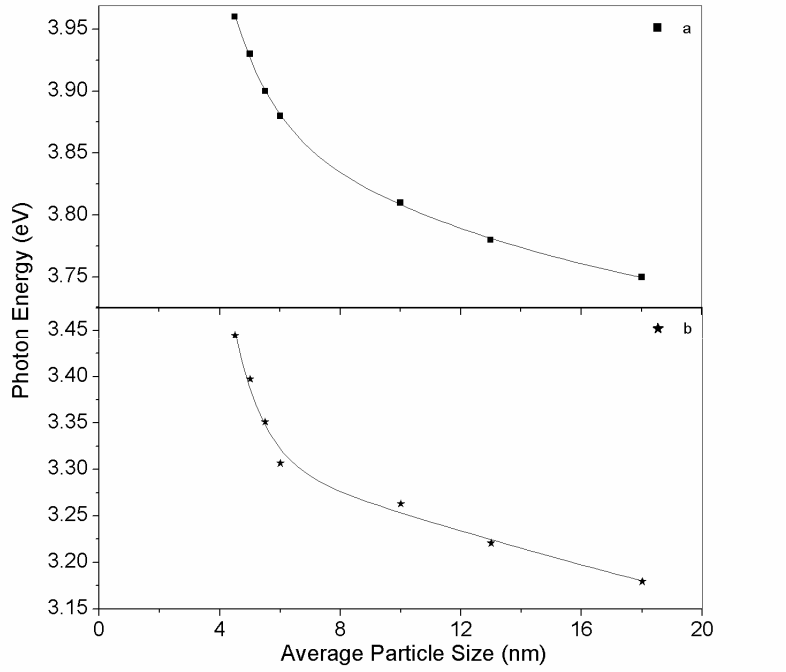

Figure 2.18:The dependence of mean particle size on

(a) *bandgap* (b) *band to band emission*

Figure 2.19 shows the fluorescence spectra of nano ZnO colloids of different particle size for an excitation wavelength of 325 nm. We have observed that with the decrease of excitation energy, the blue band peaks get suppressed and UV and green fluorescence peak becomes dominant at larger particle size[29]. The transitions from different excited states of excitons may be weakened at this higher excitation wavelength and a broad visible emission due to surface defect states become more pronounced at 325 nm excitation wavelength for ZnO colloids of size 18 nm.

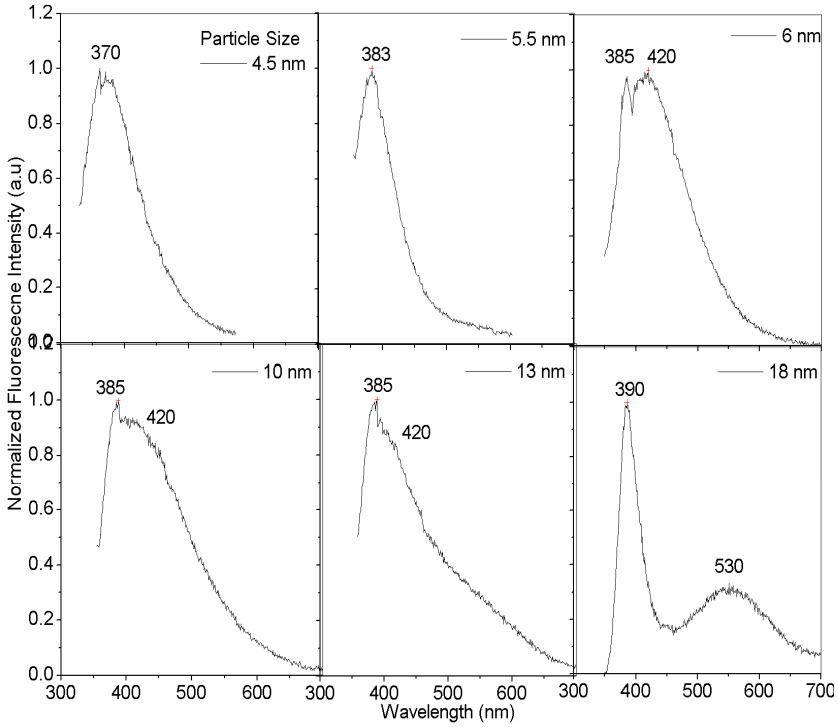

Figure 2.19: Fluorescence spectra of nano ZnO colloids of different particle size for an excitation wavelength of 325 nm

2.7.6 Visible emission

In contrast to the UV spectra, visible fluorescence spectra of ZnO particles are sensitive to the preparation procedure (and, therefore, to

environmental conditions). The well-known green fluorescence at 510 ± 50 nm appeared in colloids with larger particle size.

In ZnO, oxygen has tightly bound 2p electrons and Zn has tightly bound 3d electrons, which sense the nuclear attraction efficiently. The first principal calculation found that the Zn_{3d} electrons strongly interact with the O_{2p} electron in ZnO[60]. Since the center energy of the green peak is smaller than the bandgap energy of ZnO, the visible emission cannot be ascribed to the direct recombination of a conduction electron in the Zn_{3d} band and a hole in the O_{2p} valence band. The green emission must be related to the localized level in bandgap. The PL of ZnO has been extensively investigated, and there is no consensus in the literature on the positions of the peaks in PL spectrum of ZnO nanostructures and thin films or on their origin.

The concept of surface fluorescence-centers seems to be more realistic for nanoparticles. Researches indicate that the surface passivation via surfactant and polymer capping is an effective method to enhance the UV emission and quench the defect-related visible photoluminescence (PL) from nanosized ZnO[35, 61]. The effect of method of preparation and surface passivation itself is an indication that the green emission is due to surface states. For the uncapped ZnO nanoparticles, there exist abundant surface defects, the valence band hole can be trapped by the surface defects and then tunnels back into oxygen vacancies containing one electron to form Vo** recombination centre. The recombination of a shallowly trapped electron with a deeply trapped hole in a Vo** centre causes visible emission[62].

$$(e\text{-}V_O^{+}) + (h\text{-}V_O^{+}) \longrightarrow (e\text{-}h) \text{ in } V_O^{**}$$

The green emission is commonly referred to a deep-level or a trap-state emission attributed to the singly ionized oxygen vacancy and the emission results from the radiative recombination of photo-generated hole

with an electron occupying the oxygen vacancy[9] and Vanheusden et al. observed a correlation between the intensities of g~1.96 electron paramagnetic resonance (EPR) peak and green PL. However, the assignment of g~1.96 signal to singly ionized oxygen vacancy is controversial. This signal was also assigned to shallow donors and its position appears to be independent on the shallow donor intensity[63]. Recently, Djurisic et al.[64] found that there is no simple relationship between the intensity of g~1.96 EPR signal and the visible PL. The green PL is observed for the samples which do not show EPR line at g~1.96, and they concluded that the most likely explanation for the green luminescence involves multiple defects and/or defect complexes and the major part of the visible emission originates from the centers at the nanostructure surface. Xu et al.[65] calculated the levels of various defects including complex defects V_o:Zn_i and V_{Zn}:Zn_i. They found no states within the gap from V_{Zn}:Zn_i, while for V_o:Zn_i two levels 1.2 and 2.4 eV above the valence band were found and is depicted in figure 2.20. So this type of defect represents a possible candidate for green emission in ZnO.

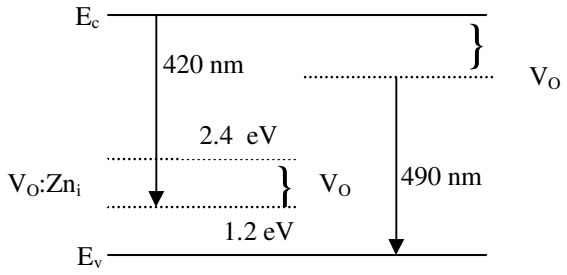

Figure 2.20: Representation of various defect levels in ZnO

ZnO is an *n*-type semiconductor and it means that most defects are Zn interstitials and oxygen vacancies. The crystal structure of ZnO as shown in figure 2.21 contains large voids which can easily accommodate interstitial

atoms[7] and the appearance of blue emission at about 420 nm when excited with 325 nm may be due to the formation of Zn interstial defects.

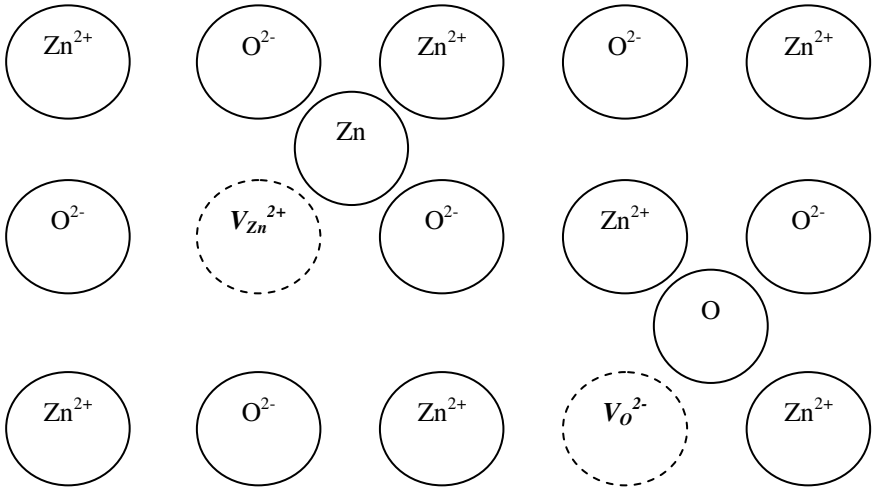

Figure 2.21: Crystal structure of ZnO

ZnO nanopowders and thin films also show green luminescence after they were annealed in oxygen, nitrogen or air[66]. The appearance of a strong green emission is ascribed to the formation of oxygen vacancy defects or antisite defects (O_{Zn}). There exists many oxygen vacancies on the surface of the ZnO annealed in Ar at 900^{o}C and shows emission peak at 490 nm while the ZnO annealed in O_2 at 900^{o}C exhibits emission peak at 530 nm. So the appearance of visible emission may have originated from the oxygen vacancy defects[66].

2.7.7 Luminescence mechanism

Figure 2.22 shows the emission mechanism of UV and visible luminescence of ZnO colloids. UV luminescence at 3.5 eV is caused by the transition from near conduction band edge to valence band[29]. As particle size increases, a shift of UV luminescence was observed from 3.5 to 3 eV because the optical energy gap decreases from 4 to 3.5 eV. The visible

luminescence in the range of 420–530 nm (2.9–2.4 eV) is mainly due to surface defect states. The UV luminescence center is not related to visible luminescence center.

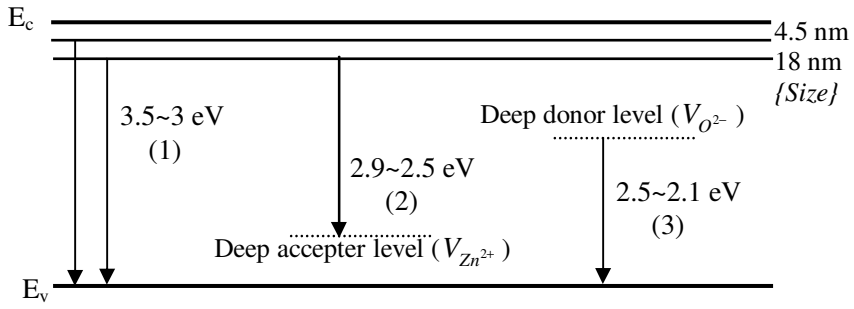

Figure 2.22:The UV and visible photoluminescence mechanism of ZnO:

(1) transition from near conduction band edge to valence band

(2) transition from near conduction band edge to deep acceptor level

(3) transition from deep donor level to valence band

Based on these results, the green luminescence of ZnO colloid is not due to the transition from near band edge to deep acceptor level in ZnO but mainly due to the transition from deep donor level by oxygen vacancies in ZnO to valence band. If green luminescence is related to the deep acceptor level, UV luminescence should have decreased as green luminescence increased. Since the UV luminescence gets suppressed in the presence of blue band, the blue luminescence is related to the deep acceptor level. These results reveal that the mechanism of blue luminescence in ZnO is by the transition from near conduction band edge to deep acceptor level.

2.8 Conclusions

In this chapter, we have highlighted the size and excitation wavelength dependence of the fluorescence behaviour in nano colloids of ZnO. The size dependent optical bandgap is systematically investigated and

there is red shift in optical bandgap with increase in particle size. The fluorescence maximum shifts towards red as the excitation wavelength is increased. This observation has been attributed to the presence of energetically different associated forms of the constituent molecules and slow rate of the excited state relaxation process in these media. The high polarity and viscosity of the medium slows down the relaxation of the excited state. In essence, the inefficient energy transfer between the upper and the lower vibrational levels of the excited state of these particles owing to short fluorescence lifetime is primarily responsible for the excitation wavelength dependent spectral shift of ZnO colloids. Fluorescence spectra consist of emissions in the UV and visible regions. Apart from the known bandgap emissions at 380 nm and impurity dominated emissions at 530 nm, emissions in the 420-490 nm range are also observed with increase in particle size. This series of peaks are related to the transition from excited state energy levels of exciton to ground state by modelling it with a particle in a box problem. The UV band has been assigned to the *bandgap* fluorescence of clusters of different sizes. This allows us to reconstruct the size distribution curves from fluorescence spectroscopy. Systematic studies on nano crystallites have indicated the presence of luminescence due to excitonic emissions when excited with 255 nm as well as significant contribution from surface defect states when excited with 325 nm. The relevant energy levels showing the transitions corresponding to the observed peaks in the emission spectrum of ZnO of particle size 18 nm under 255 nm excitation are calculated. The luminescence mechanism is discussed.

2.9 References

1 S A Studenikin, M Cocivera, W Kellner and H Pascher; "*Band-edge photoluminescence in polycrystalline ZnO films at 1.7 K*", J. Lumin. **91**, 223 (2000)

2 S. Nakamura, *The Blue Laser Diode* (Springer, New York, 1997)

3 D. C. Reynolds, D. C. Look and B. Jogai; "*Optically pumped ultraviolet lasing from*

ZnO", Solid State Commun. **99**, 873 (1996)

4 Zhong Ling Wang; "*Zinc oxide nanostructures: growth, properties and applications*", J. Phys.: Condens. Matter. **16,** R829 (2004)

5 Louis Brus; "*Electronic wave functions in semiconductor clusters: experiment and theory*", *J. Phys. Chem.* **90**, 2555 (1986)

6 R M Nyffenegger et.al."*A Hybrid Electrochemical/Chemical Synthesis of Zinc Oxide Nanoparticles and Optically Intrinsic Thin Films*", Chem. Mater. **10,** 1120 (1998)

7 L. V. Azaroff, *Introduction to Solids* (McGraw–Hill, New York, 1960)

8 K. Vanheusden, W. L. Warren, C. H. Seager, D. R. Tallant, J. A. Voigt, and B. E. Gnade; "*Mechanisms behind green photoluminescence in ZnO phosphor powders*", J. Appl. Phys. **79**, 7983 (1996)

9 W. Li, D. Mao, F. Zhang, X. Wang, X. Liu, S. Zou, Y. Zhu, Q. Li, and J. Xu; "*Characteristics of ZnO:Zn phosphor thin films by post-deposition annealing*", Nucl. Instrum. Methods Phys. Res. B, **169**, 59 (2000)

10 T Voddmeyer, D J Katsikas, M Giersig, I G Popovic, K Diesner, A Chemseddine, A Eychmuller and H Weller; "*Luminescent properties of local atomic order of Er^{3+} and Yb^{3+} ions in aluminophosphate glasses*" J. Appl. Phys. **90**, 265 (2001)

11 H Yu, J Li, R A Loomis, P C Gibbons, L W Wang and W E Buhro; "*Cadmium selenide quantum wires and the transition from 3D to 2D confinement*" J. Am. Chem. Soc. **125**, 16168 (2003)

12 S Baskoutas and A F Terzis; "*Size-dependent bandgap of colloidal quantum dots*", J. Appl. Phys. **99**, 013708 (2006)

13 S Baskoutas; "*Excitons and charged excitons in InAs nanorods*" Chem. Phys. Lett. **404**, 107 (2005)

14 L E Brus; "*Electron–electron and electron-hole interactions in small semiconductor crystallites: The size dependence of the lowest excited electronic state*" J. Chem. Phys. **80**, 4403 (1984)

15 Efros A L, "*Interband absorption of light in semiconductor spheres*", Sov. phys. semicond.**16**, 772 (1982)

16 Y Kayanuma and H Momiji; "*Incomplete confinement of electrons and holes in microcrystals*" Phys. Rev. B **41**, 10261 (1990)

17 K K Nanda, F E Kruis and H Fissan; "*Effective mass approximation for two extreme semiconductors: Bandgap of PbS and CuBr nanoparticles*" J. Appl. Phys. **95**, 5035 (2004)

18 G Pellegrini, G Mattei and P Mazzoldi, J. Appl. Phys. **97**, 073706 (2005)

19 Xia J B; "*Electronic structures of zero-dimensional quantum wells*", Phys Rev. **40**, 8500 (1989)

20 Grigorian G B, Kazaryan E M, Efros A L and Yazeva T V; "*Quantized holes and the absorption edge in semiconductor nanocrystals with a complex valence band structure*",

Sov. Phys. Solid. State **32**, 1031 (1990)

21 Vahala K J and Sercel P C; "*Application of total angular momentum basis quantum dot structure*", Phys. Rev.Lett, **65**, 239 (1990)

22 Ekimov A L et.al.; "*Absorption and intensity dependent photoluminescence measurements on CdSe quantum dots: assignment of the first electronic transitions*", J. Opt. Soc. Am. B **10**, 100 (1993)

23 Richard T, Lefebvre P, Mathieu H and Allegre J; "*Effects of finite spin-orbit splitting on optical properties of spherical semiconductor quantum dots*", Phys. Rev. B **53**, 7287 (1996)

24 S Baskoutas and A F Terzis; "*Size dependent exciton energy of various technologically important colloidal quantum dots*" Mater. Sci. Eng. B (2007), doi:10.1016/j.mseb.2007.09.041

25 Chepic D I, Efros A L, Ekimov A I, Ivanov M G, Kharchenko V A, Kudriavtsev I A and Yazeva T V; "*Auger ionization of semiconductor quantum dots in a glass matrix*", J. of Lum. **47**, 113 (1990)

26 Klimov V I, Mikhailovsky A A, McBranch D W, Leatherrdale C A, Bawendi M G; "*Quantization of multiparticle Auger rates in semiconductor quantum dots*", Science **287**, 1011 (2000)

27 Didier Jezequel, Jean Guenot, Noureddine Jouini, Fernand Fievet; "*Submicrometer zinc oxide particles: Elaboration in polyol medium and morphological characteristics*", *J.Mater.Res.*, **10**, 77, (1995)

28 Eric W. Seelig, Betty Tang, Alexey Yamilov, Hui Cao and R. P. H. Chang; "*Self-assembled 3D photonic crystals from ZnO colloidal spheres*", Materials Chemistry and Physics, **80**, 257 (2002)

29 Litty Irimpan et.al.; '*Size dependent fluorescence spectroscopy of nanocolloids of ZnO*', J. Appl. Phys. **102**, 063524 (2007)

30 Litty Irimpan, Bindu Krishnan, A Deepthy, V P N Nampoori and P Radhakrishnan; J. Phys. D: Appl. Phys. **40,** 5670 (2007)

31 S. Monticone, R. Tufeu, and A.V. Kanaev; "*Complex Nature of the UV and Visible Fluorescence of Colloidal ZnO Nanoparticles*", J.Phys.Chem B, **102**, 2854 (1998)

32 D. Luna-Moreno, E. De la Rosa-Cruz, F. J. Cuevas, L. E. Regalado, P. Salas, R. Rodríguez and V. M. Castano; "*Refractive index measurement of pure and Er^{3+}-doped ZrO_2–SiO_2 sol–gel film by using the Brewster angle technique* ", *Opt. Mat*., **19**, 275 (2002)

33 Ranjani Viswanatha, Sammer Sapra, B.Satpati, P.V.Satyam, B.N.Dev, D.D Sharma; "*Understanding the quantum size effects in ZnO nanocrystals*", *J.Mater.Chem,***14**, 661,(2004)

34 1999 JCPDS-International Centre for Diffraction Data.

35 Lin Guo, Shihe Yang, Chunlei Yang, Ping Yu, Jiannong Wang, Weikun Ge, and George

K. L. Wong; "*Highly monodisperse polymer-capped ZnO nanoparticles: Preparation and optical properties*", *Appl. Phys. Lett.,* **76** 2901 (2000)

36 V L Colvin, A P Alivisatos and J.G. Tobin; "*Valence-band photoemission from a quantum-dot system*", Phys. Rev. Lett., **66**, 2786 (1991)

37 S Sapra and D D Sarma; "*Evolution of the electronic structure with size in II-VI semiconductor nanocrystals*", Phys. Rev. B **69**, 125304 (2004)

38 W. Zhang, H. Wang, K.S. Wong, Z.K. Tang, G.K.L. Wong, J. Ravinder, "*Third-order optical nonlinearity in ZnO microcrystallite thin films*", Appl. Phys. Lett; **75**, 3321 (1999)

39 Rana Karmakar and Anunay Samanta; J. Phys. Chem. A, **107,** 7340 (2003)

40 S Saha, Prasun K. Mandal and Anunay Samanta; "*Solvation dynamics of Nile Red in a room temperature ionic liquid using streak camera*", Phys. Chem. Chem. Phys., **6**, 3106 (2004)

41 Debdeep Chakrabarty, Debabrata Seth, Anjan Chakraborty, and Nilmoni Sarkar; "*Dynamics of Solvation and Rotational Relaxation of Coumarin 153 in Ionic Liquid Confined Nanometer-Sized Microemulsions*", J. Phys. Chem. B, **109,** 5753 (2005)

42 Prasun K. Mandal and Anunay Samanta; "*Fluorescence Studies in a Pyrrolidinium Ionic Liquid: Polarity of the Medium and Solvation Dynamics*", J. Phys. Chem. B, **109**, 15172 (2005)

43 Aniruddha Paul, Prasun Kumar Mandal and Anunay Samanta; "*How transparent are the imidazolium ionic liquids? A case study with 1-methyl-3-butylimidazolium hexafluorophosphate, [bmim][PF_6]* ", Chem. Phys. Lett. **402**, 375 (2005)

44 Aniruddha Paul, Prasun Kumar Mandal, and Anunay Samanta; "*On the Optical Properties of the Imidazolium Ionic Liquids*", J. Phys. Chem. B **109**, 9148 (2005)

45 Sang-Woo Kim, Shizuo Fujita, Shigeo Fujita; "*Self-organized ZnO quantum dots on SiO_2/Si substrates by metalorganic chemical vapor deposition*", A*ppl. Phys. Lett.* **81** 5036 (2002)

46 Birks JB; "*Photophysics of Aromatic Molecules*", Wiley-Interscience: London, 1970

47 Alexander P. Demchenko; "*The red-edge effects: 30 years of exploration*", Luminescence, **17**, 19 (2002)

48 Joseph R. Lakowicz and Susan Keating-Nakamoto; "*Red-edge excitation of fluorescence and dynamic properties of proteins and membranes*", Biochemistry, **23**, 3013 (1984)

49 Bernard Valeur and Gregorio Weber; "*Anisotropic rotations in 1-naphthylamine. Existence of a red-edge transition moment normal to the ring plane*", Chem. Phys. Lett., **45**, 140 (1977)

50 G Weber and M Shinitzky; "*Failure of Energy Transfer between Identical Aromatic Molecules on Excitation at the Long Wave Edge of the Absorption Spectrum*", Proc. Natl. Acad. Sci. U S A, **65**, 823 (1970)

51 K. Itoh and T. Azumi; "*Shift of emission band upon excitation at the long wavelength*

absorption edge. 1. A preliminary survey for quinine and related compounds", Chem. Phys. Lett., **22**, 395 (1973)

52 Ken-ichi Itoh and Tohru Azumi; "*Shift of the emission band upon excitation at the long wavelength absorption edge. II. Importance of the solute–solvent interaction and the solvent reorientation relaxation process*", J. Chem. Phys., **62**, 3431 (1975)

53 Lakowicz J R; "*Principles of Fluorescence Spectrosopy"*, Plenum Press: New York, 1999

54 Amitabha Chattopadhyay and Sushmita Mukherjee; "*Red Edge Excitation Shift of a Deeply Embedded Membrane Probe: Implications in Water Penetration in the Bilayer*", *J. Phys. Chem. B*, **103**, 8180 (1999)

55 H. S. Bhatti, Atul Gupta, N. K. Verma and Sunil Kumar; "*Optical characterization of ZnO nanobelts*", Journal of Materials Science: Materials in Electronics, **17**, 4 (2006)

56 D W Bahnemann, C Kormann and M R. Hoffmann; "*Preparation and Characterization of Quantum Size ZnO: A Detailed Spectroscopic Study*", *J. Phys. Chem., **91**,* 3789 (1987)

57 Ian K. Smith, Stuart R. Andrews, Graham Williams and Paul A. Holmes; *J. Mater. Chem.***, 6,** 539 (1996)

58 A Dvornikov, Y Liang, Peter Rentzepis; "*Dependence of the fluorescence of a composite photochromic molecule on structure and viscosity*", J. Mater. Chem., **15**, 1072 (2005)

59 Kim S W, Fujita S and Fujita S; "*Self-organized ZnO quantum dots on SiO_2/Si substrates by metalorganic chemical vapor deposition*", A*ppl. Phys. Lett.,* **81** 5036 (2002)

60 P. Schroer, P. Kruger, J. Pollmann; "*First-principles calculation of the electronic structure of the wurtzite semiconductors ZnO and ZnS*", Phys. Rev. B, **47,** 6971 (1993)

61 Fonoberov V A and Balandin A; "*Origin of UV photoluminescence in ZnO quantum dots: Confined excitons versus surface-bound impurity exciton complexes*", *Appl. Phys. Lett.,* **85,** 5971 (2004)

62 van Dijken A, Meulenkamp E A, Vanmaekelbergh D and Meijerink A; "*The Kinetics of the Radiative and Nonradiative Processes in Nanocrystalline ZnO Particles upon Photoexcitation*", *J. Phys. Chem.* B, **104,** 1715 (2000)

63 N.Y. Garces, N.C. Giles, L.E. Halliburton, G. Cantwell, D.B. Eason, D.C. Reynolds, L.C. Look; "*Production of nitrogen acceptors in ZnO by thermal annealing*", Appl. Phys. Lett. **80,** 1334 (2002)

64 A.B. Djurisic et.al.; "*Photoluminescence and Electron Paramagnetic Resonance of ZnO Tetrapod Structures*", Adv. Funct. Mater. **14,** 856 (2004)

65 P.S. Xu, Y.M. Sun, C.S. Shi, F.Q. Xu, H.B. Pan; "*The electronic structure and spectral properties of ZnO and its defects*", Nucl. Instrum. Methods B; **199,** 286 (2003)

66 J.Z. Wang, G.T. Du, Y.T. Zhang, B.J. Zhao, X.T. Yang, D.L. Liu; "*Luminescence properties of ZnO films annealed in growth ambient and oxygen* ", J. Crystal Growth., **263**, 269 (2004)